International Journal of Mechanical, Industrial and Aerospace Sciences
ISSN: 2517-9950
Vol:8, No:11, 2014

In situ Modelling of Lateral-Torsional Vibration of a Rotor-Stator with Multiple Parametric Excitations

B. X. Tchomeni, A. A. Alugongo, L. M. Masu

***Abstract*—**This paper presents a 4-DOF nonlinear model of a cracked de Laval rotor-stator system derived based on Energy Principles. The model has been used to simulate coupled torsional-lateral response of the faulty system with multiple parametric excitations; rotor-stator-rub, a breathing transverse crack, eccentric mass and an axial force. Nonlinearity of a "breathing" crack is incorporated in the model using a simple hinge mechanism suitable for a shallow crack. Response of the system while passing via its critical speed with intermittent rotor-stator rub is analyzed. Effects of eccentricity with phase and acceleration are investigated. Features of crack, rub and eccentricity in vibration response are explored for condition monitoring. The presence of a crack and rub are observable in the power spectrum despite excitations by an axial force and rotor unbalance. Obtained results are consistent with existing literature and could be adopted into rotor condition monitoring strategies.

***Keywords*—**Axial force, Crack, Nonlinear, Rotor-Stator, Rub.

I. Introduction

DESIGN and vibration control of rotating machines require prediction of dynamic characteristics; resonance thresholds, stability limits, participating modes and interactions of machine parts in the sub-critical and in super-critical regimes [1]. Rotor-stator rub involves several phenomena; impact, friction, and stiffness modification among others. Rub forces significantly affect system's stability limits [2]. Most of the reported research analyzes rotor stability using various models and simulation techniques [3]-[5].

A rotor-stator-rub diagnostic model and dynamic characteristics to be observed are given in [6]. This model has gained a wide application to-date [7].

A model of torsional-lateral vibrations with rotor-to-stator rub was proposed in [7]. Rub was simulated as elastic impact-contact, and rub forces represented by friction coefficient, normal and tangential forces at rotor-stator contact point.

A multi-mass model to assess the degree to which chaos gets distributed in a rotor- stator system was developed in [8].

An analysis of rotor-stator rub done on system bifurcation using various damping ratios, Poincare map and FFT spectrum in [9] revealed predominance of rub at the bottom of the clearance circle at a low rotor speed. A quasi-periodic model of a rotor with a bearing clearance was derived by Harmonic Balance Method in [10]. A subsequent stability analysis revealed system's nonlinear features.

Rotor-stator rub was modelled and stiffening of rotor shaft quantitatively investigated in [11]. Change in transient stiffness served as a sufficient indicator of rub-impact.

Rotor-stator rub and the often neglected axial force effect in a Lagrangian formulation was analyzed by FFT [12]. Simulation at a constant shaft speed failed to indicate most of the nonlinear phenomena. At non-uniform speed, nonlinear features including bifurcation and chaos were observed.

Rotor vibration condition monitoring focuses on acceleration-deceleration phase, passage via critical speed, and coupling of diverse vibration modes [14].

The current paper focus on the analysis of coupled lateral-torsional vibrations of unbalanced rotor-stator system with multiple parametric excitations; rub, a breathing transverse crack, and an axial force. For the analysis, the model in [7], [12] is extended following Energy principles. A layout of the physical system under consideration is shown in Fig. 1.

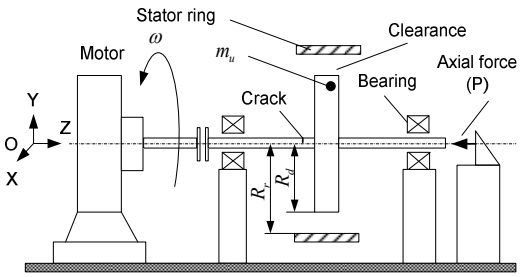

Fig. 1 Motor-shaft-disc –stator-transverse crack and axial force [P]

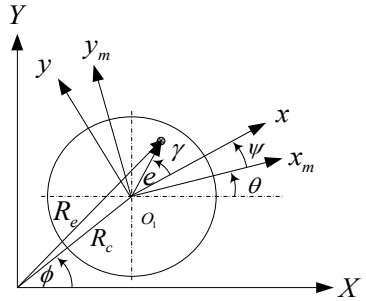

Fig. 2 Section view of disc on the shaft in inertial, rotating and motor coordinates (X, Y), (x, y), (x_m, y_m) respectively

II. Mathematical Model of the Study

The kinetic energy equation of the system in of Fig. 2 is [7]:

B. X. Tchomeni, postgraduate student, and A. A. Alugongo Mech. Eng Dept., are with the Vaal University of Technology, Vanderbijlpark, South Africa, (phone:+27- 169509302; fax: +27-169509797; e-mail: bmignon@gmail.com, alfayoa@vut.ac.za).

L. M. Masu, is with Mech. Eng Dept., Vaal University of Technology, Vanderbijlpark, South Africa (phone: +27- 169506817; fax: +27-169509797; e-mail:leonard@vut.ac.za).

$$U_D = \frac{1}{2}M\left(\dot{X}^2 + \dot{Y}^2\right) + \frac{1}{2}J_D\left(\dot{\theta} + \dot{\psi}\right)^2 + \frac{1}{2}J_M\dot{\theta}^2 + \frac{1}{2}m_u\dot{R}_e^T\dot{R}_e \quad (1)$$

J_D, J_M, θ, ψ and $\dot{R}_e$ respectively are, disc-mass moment of inertia, motor-mass moment of inertia, rigid-body rotation, twist about Z-axis and velocity vector of m_u. Upon differentiating R_e with respect to time and making appropriate substitution as in [7], simplification of (1) yields:

$$U_D = \frac{1}{2}(m_u + M)\left(\dot{X}^2 + \dot{Y}^2\right) + \frac{1}{2}m_u e^2\dot{\theta}^2(1+\psi^2) + \frac{1}{2}m_u e^2\dot{\psi}^2 - m_u\dot{X}\dot{\theta}[(e_x - \psi e_y)sin\theta + (e_x\psi + e_y)cos\theta] + m_u\dot{Y}\dot{\theta}[(e_x - \psi e_y)cos\theta - (e_x\psi + e_y)sin\theta] - m_u\dot{X}\dot{\psi}(e_x sin\theta + e_y cos\theta) + m_u\dot{Y}\dot{\psi}(e_x cos\theta - e_y sin\theta) + m_u e^2\dot{\psi}\dot{\theta} + \frac{1}{2}J_M\dot{\theta}^2 + \frac{1}{2}J_D\left(\dot{\theta} + \dot{\psi}\right)^2 \quad (2)$$

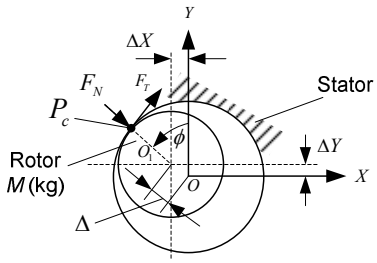

Fig. 3 Geometry of rotor, rubbing impact force and a clearance

III. Forces Acting on the Rotor's Shaft

The shaft deflects under, torque, crack, unbalance, axial force and rub. Using Fig. 3, the position of shaft center and rotor-stator clearance are, $\vec{R} = X\vec{\imath} + \overrightarrow{Yj}$, and $\Delta = R_r - R_s$. Friction force F_T, acts at the contact point. Contact occurs when,

$$R - \Delta \geq 0 \quad (3)$$

When $R < \Delta$, contact ceases and F_T vanishes. The value of R at an arbitrary point P_c, is

$$R = \sqrt{(X - \Delta X)^2 + (Y - \Delta Y)^2}. \quad (4)$$

The position of P_c relative to point O in the (X, Y) frame is,

$$\overrightarrow{R} = (\Delta + \Delta_{XY})(cos\emptyset\,\vec{\imath} + sin\emptyset\,\vec{\jmath}) \quad (5)$$

where

$$X = (\Delta_X + \Delta)cos\emptyset\ ;\ Y = (\Delta_Y + \Delta)sin\emptyset \quad (6)$$

$$tan\emptyset = \frac{Y}{X} \quad (7)$$

Therefore,

$$F_N = K_s(R - \Delta); \quad F_T = -\mu K_s(R - \Delta) \quad (8)$$

F_N and μ respectively are, radial component due to impact and friction coefficient. The lateral forces in X and Y directions are:

$$F_X = -F_N cos\emptyset + F_T sin\emptyset;\ F_Y = -F_N sin\emptyset - F_T cos\emptyset \quad (9)$$

In Cartesian coordinates, the forces are expressed as,

$$F_X = -K_s\left(1 - \frac{\Delta}{R}\right)X + K_s\left(1 - \frac{\Delta}{R}\right)\mu Y \quad (10)$$

$$F_Y = -K_s\left(1 - \frac{\Delta}{R}\right)\mu X - K_s\left(1 - \frac{\Delta}{R}\right)Y \quad (11)$$

IV. Potential Energy Expression

The system elastic strain energy is:

$$V = \frac{1}{2}K_{XX}X^2 + \frac{1}{2}K_{YY}Y^2 + \frac{1}{2}K_{\psi\psi}\psi^2 \quad (12)$$

A high rotor speed excites axial and lateral vibrations which affect bending stiffness as given in [12].

$$K_{XX} = K_{YY} = K_b - \frac{P\pi^2}{2L} - \frac{F_\psi\pi^3}{2L^2}\ ; \quad (13)$$

K_b, P and F_ψ correspondingly are, modal stiffness of first bending mode, fluctuating axial force and axial torque. In this paper P and F_ψ are prescribed a priori as in [15].

$$P = P_0 + P_f sin\theta, \quad F_\psi = T_0 + T_f sin\theta \quad (14)$$

P_f, T_f and θ are amplitudes and rotation angle respectively. The system Rayleigh's dissipation function is expressed as,

$$G = \frac{1}{2}C_{XX}\dot{X}^2 + \frac{1}{2}C_{YY}\dot{Y}^2 + \frac{1}{2}C_{\psi\psi}\dot{\psi}^2 \quad (15)$$

V. System Equation of Motion

Substituting (10)-(15) into Lagrange's equation, performing requisite differentiation and manipulations, yields:

$$\begin{bmatrix} m_{\theta\theta} & m_{\theta\psi} & m_{\theta X} & m_{\theta Y} \\ m_{\psi\theta} & m_{\psi\psi} & m_{\psi X} & m_{\psi Y} \\ m_{X\theta} & m_{X\psi} & m_{XX} & 0 \\ m_{Y\theta} & m_{Y\psi} & 0 & m_{YY} \end{bmatrix}\begin{Bmatrix} \ddot{\theta} \\ \ddot{\psi} \\ \ddot{X} \\ \ddot{Y} \end{Bmatrix} + \begin{bmatrix} 0 & 0 & 0 & 0 \\ 0 & C_{\psi\psi} & 0 & 0 \\ 0 & 0 & C_{XX} & C_{XY} \\ 0 & 0 & C_{YX} & C_{YY} \end{bmatrix}\begin{Bmatrix} \dot{\theta} \\ \dot{\psi} \\ \dot{X} \\ \dot{Y} \end{Bmatrix} + \begin{bmatrix} 0 & 0 & 0 & 0 \\ 0 & K_{\psi\psi} & 0 & 0 \\ 0 & 0 & K_{XX} & K_{XY} \\ 0 & 0 & K_{YX} & K_{YY} \end{bmatrix}\begin{Bmatrix} \theta \\ \psi \\ X \\ Y \end{Bmatrix} + \begin{Bmatrix} Q_\theta \\ 0 \\ Q_X \\ Q_Y \end{Bmatrix} = \begin{Bmatrix} F_\theta \\ F_\psi \\ F_X \\ F_Y \end{Bmatrix} \quad (16)$$

Elements referred to in (16) are as set out in [7].

VI. Rotor Model with a Transverse Crack

A hinge mechanism is incorporated in the shaft to provide for local flexibility of a breathing crack [4]. Shear stresses are neglected, Saint-Venant's principle observed [8] and [13] used on (16) yielding the following equation of motion:

$$\begin{bmatrix} m_{\theta\theta} & m_{\theta\psi} & m_{\theta X} & m_{\theta Y} \\ m_{\psi\theta} & m_{\psi\psi} & m_{\psi X} & m_{\psi Y} \\ m_{X\theta} & m_{X\psi} & m_{XX} & 0 \\ m_{Y\theta} & m_{Y\psi} & 0 & m_{YY} \end{bmatrix}\begin{Bmatrix} \ddot{\theta} \\ \ddot{\psi} \\ \ddot{X} \\ \ddot{Y} \end{Bmatrix} + \begin{bmatrix} 0 & 0 & 0 & 0 \\ 0 & C_{\psi\psi} & 0 & 0 \\ 0 & 0 & C_{XX} & C_{XY} \\ 0 & 0 & C_{YX} & C_{YY} \end{bmatrix}\begin{Bmatrix} \dot{\theta} \\ \dot{\psi} \\ \dot{X} \\ \dot{Y} \end{Bmatrix} + \begin{bmatrix} 0 & 0 & 0 & 0 \\ 0 & K_{\psi\psi} & 0 & 0 \\ 0 & 0 & K_{XX} & K_{XY} \\ 0 & 0 & K_{YX} & K_{YY} \end{bmatrix}\begin{Bmatrix} \theta \\ \psi \\ X \\ Y \end{Bmatrix} - \frac{1}{2}f(t)\Delta k_{xx} \times \begin{bmatrix} 0 & 0 & 0 & 0 \\ 0 & 0 & 0 & 0 \\ 0 & 0 & 1 - cos2\theta & sin2\theta \\ 0 & 0 & sin2\theta & 1 + cos2\theta \end{bmatrix}\begin{Bmatrix} 0 \\ 0 \\ Y_S \end{Bmatrix} + \begin{Bmatrix} Q_\theta \\ 0 \\ Q_X \\ Q_Y \end{Bmatrix} = \begin{Bmatrix} F_\theta \\ F_\psi \\ F_X \\ F_Y \end{Bmatrix} \quad (17)$$

where,Δk_{xx} ,K_0, and $f(\theta)$ are respectively, change in stiffness in the weaker axis due to the crack, uncracked shaft stiffness and steering function.$f(\theta)$is taken from [13].

VII. Numerical Simulation And Discussion

The system parameters in [7] are adopted for simulation. Velocity and torque time histories are given a priori in Figs. 4 (a), (b). Equation (17) is numerically solved on diverse hypothesis by a Modified Runge–Kutta algorithm in MATLAB giving X, Y, θ at time step,$\Delta_t = 0.001s$, between $t = 0\ s$,and $t = 20\ s$.

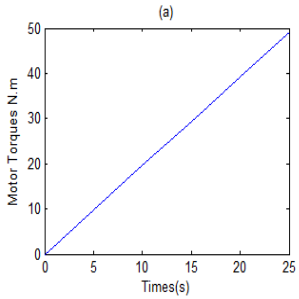

Fig. 4 (a) Torque-Time history

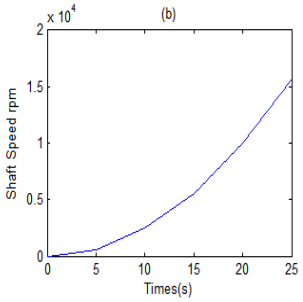

Fig. 4 (b) Shaft speed history

VIII. Lateral Motion and Axial Forces Effects

For this simulation, a reduced order model refer to (17) is used in the form

$$\begin{bmatrix} m_{\theta\theta} & m_{\theta X} & m_{\theta Y} \\ m_{X\theta} & m_{XX} & 0 \\ m_{Y\theta} & 0 & m_{YY} \end{bmatrix} \begin{Bmatrix} \ddot{\theta} \\ \ddot{X} \\ \ddot{Y} \end{Bmatrix} + \begin{bmatrix} 0 & 0 & 0 \\ 0 & C_{XX} & 0 \\ 0 & 0 & C_{YY} \end{bmatrix} \begin{Bmatrix} \dot{\theta} \\ \dot{X} \\ \dot{Y} \end{Bmatrix} + \begin{bmatrix} 0 & 0 & 0 \\ 0 & K_{XX} & 0 \\ 0 & 0 & K_{YY} \end{bmatrix} \begin{Bmatrix} \theta \\ X \\ Y \end{Bmatrix} = \frac{1}{2} f(t) \Delta k_{xx} \begin{bmatrix} 0 & 0 & 0 \\ 0 & 1-cos2\theta & sin2\theta \\ 0 & sin2\theta & 1+cos2\theta \end{bmatrix} \begin{Bmatrix} 0 \\ 0 \\ Y_{st} \end{Bmatrix} - \begin{Bmatrix} Q_\theta \\ Q_X \\ Q_Y \end{Bmatrix} + \begin{Bmatrix} T_f \\ 0 \\ 0 \end{Bmatrix} \quad (18)$$

X,Y and θ are evaluated on passing via critical speed with and without a crack. Cross-coupling stiffness and damping coefficients adopted are, $C_{XY} = C_{YX}$=$K_{XY} = K_{YX} = 0$

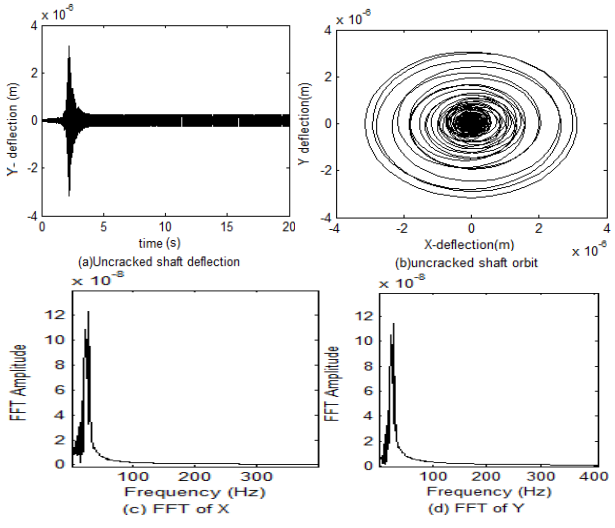

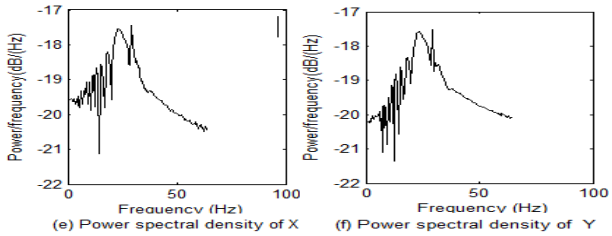

Fig. 5 (A) Dynamic response, no torsional flexibility, rub, crack but axial force, $\Delta K_\xi/K_b$=0, ψ =0, P=2kN: (a) Vertical deflection of uncracked shaft; (b) Rotor response orbit; (c) X-Lateral frequency; (d) Y-lateral frequency; (e) X-Lateral power spectra; (f) Y-Lateral power spectra

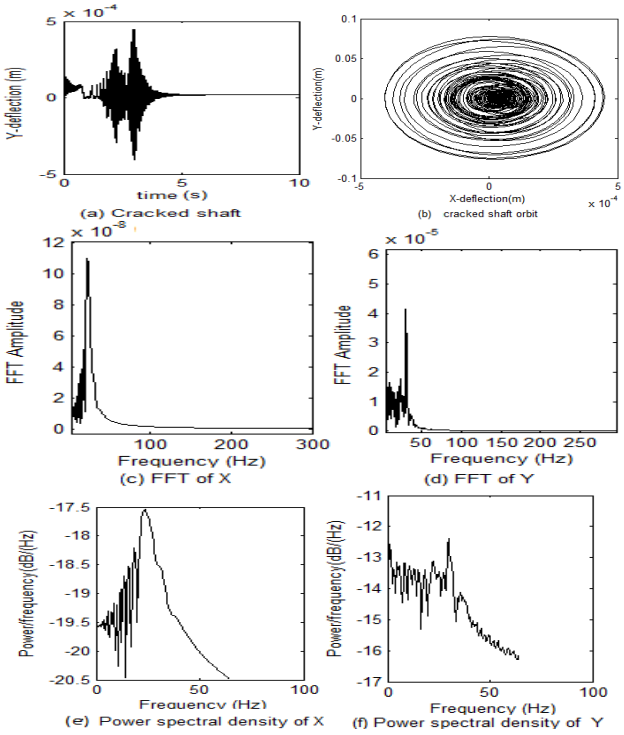

Fig. 5 (B) Dynamic response of cracked rotor via the critical speed, with axial force, and no rub, $\Delta K_\xi/K_b$=0.9542, P=2 kN: (a) Y- cracked shaft deflection; (b) Rotor response orbit; (c) X-Lateral frequency; (d) Y-Lateral frequency; (e) X-Power spectral density; (f) Y-Power spectral density.

Comparing the orbits in Figs. 5 (A) and (B), it is apparent that, the breathing crack is a source of extra evolution in the vibration response, especially when the rotating speed falls in the neighborhood of half of the system critical speed.

The maximum orbit amplitudes in Fig. 5 (B) (b) are modified from $R_1 = 3.167 \times 10^{-6} m$ to $R_2 = 5.025 \times 10^{-4} m$ when the speed changes respectively from $\omega_1 = 1132.27\ rpm$ in Fig. 5 (A) (c) to $\omega_2 = 1855.43\ rpm$ in Fig. 5 (B) (c) i.e. from a healthy to a cracked shaft. The cracked shaft is characterized by presence of strong tightening loops.

In Fig. 5 (B) (c), the frequency amplitudes where the inside orbit loop is higher is present, is greater than that of a rotor with small axial force in Fig. 5 (A) (c).

Fig. 5 (B) (d) reveals that a high vibrational level is reached by order 1 harmonic at $23.46\ Hz$.

Vibration in the axial direction does not provide information on the presence of the crack. Axial force causes a variation in power density spectrum and gives resonance when increased to 6.0 kN. Increasing axial force to 12kN intensifies the vibration and a third resonance peak is observed in Fig. 6 (a). The abrupt change in the inside orbit loop indicates a breathing crack.

IX. Rub Under Axial Force and a Crack

The reduced order model equation for this case is,

$$\begin{bmatrix} m_{\theta\theta} & m_{\theta X} & m_{\theta Y} \\ m_{X\theta} & m_{XX} & 0 \\ m_{Y\theta} & 0 & m_{YY} \end{bmatrix} \begin{Bmatrix} \ddot{\theta} \\ \ddot{X} \\ \ddot{Y} \end{Bmatrix} + \begin{bmatrix} 0 & 0 & 0 \\ 0 & C_{XX} & 0 \\ 0 & 0 & C_{YY} \end{bmatrix} \begin{Bmatrix} \dot{\theta} \\ \dot{X} \\ \dot{Y} \end{Bmatrix} + \begin{bmatrix} 0 & 0 & 0 \\ 0 & K_{XX} & 0 \\ 0 & 0 & K_{YY} \end{bmatrix} \begin{Bmatrix} \theta \\ X \\ Y \end{Bmatrix} = -\begin{Bmatrix} Q_\theta \\ Q_X \\ Q_Y \end{Bmatrix} + \begin{Bmatrix} F_\theta \\ F_X \\ F_Y \end{Bmatrix} + \left(\frac{1}{2} f(t) \Delta k_{xx} \begin{bmatrix} 0 & 0 & 0 \\ 0 & 1-cos2\theta & sin2\theta \\ 0 & sin2\theta & 1+cos2\theta \end{bmatrix} \begin{Bmatrix} 0 \\ 0 \\ Y_{st} \end{Bmatrix} \right) \quad (19)$$

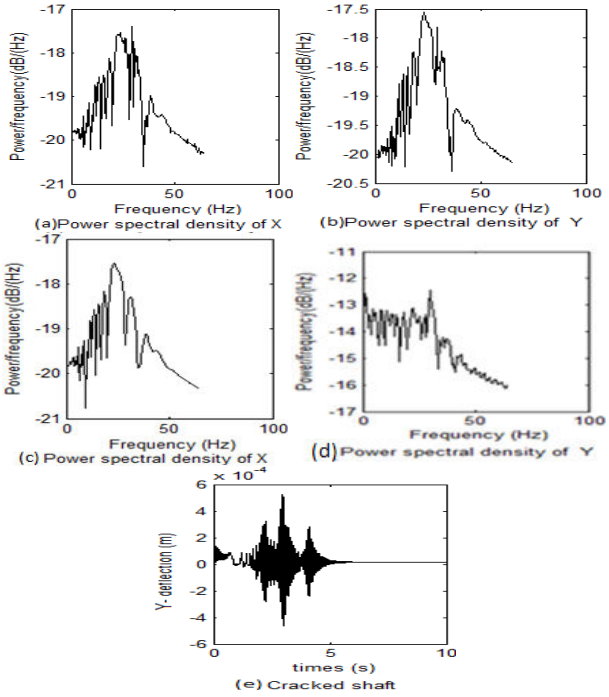

Fig. 6 (a), (b). Variation of power spectrum density for uncracked (c), (d). cracked shaft deflection at axial force P=6 kN. (e) Shaft orbit trajectory at large axial force P=12kN

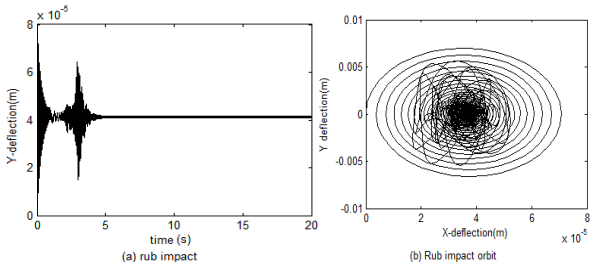

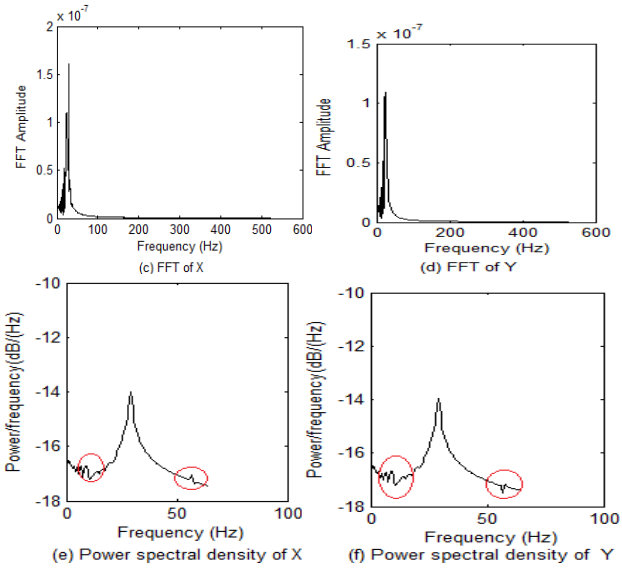

Fig. 7 (A) Rotor lateral-rotor response without torsional deformation, with rub, axial force: $\Delta K_\xi/K_b=0$, $\psi=0$. P=2000N (a) Vertical uncracked shaft deflection (b) Rotor response orbit, (c) X-Lateral frequency signal, (d) Y-Lateral frequency signal, (e) X-Lateral power spectral density (f), Y-Lateral power spectral

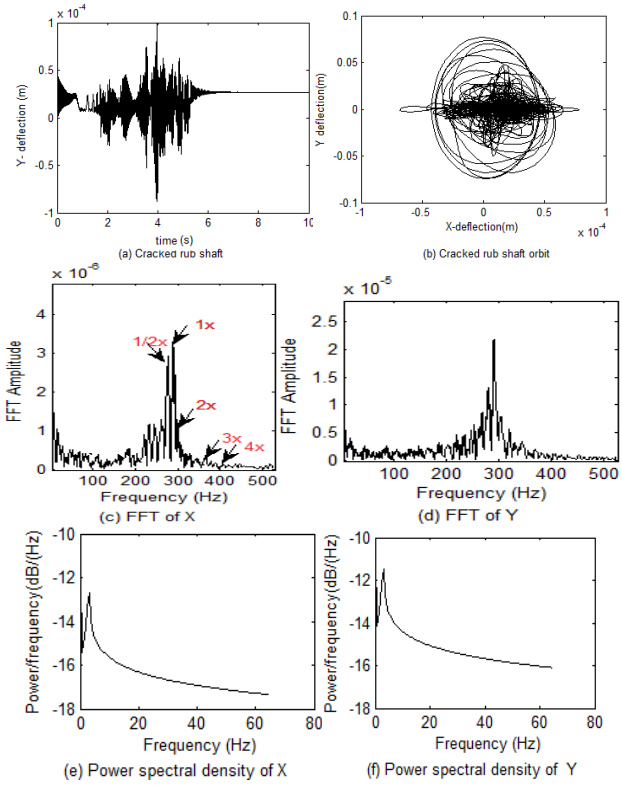

Fig. 7 (B) Rotor system response of the lateral-rotor model without torsional flexibility, with rotor-to-stator rub, small axial force and crack, $\Delta K_\xi/K_b=0.9542$, $\Delta = 2.65 \times 10^{-7}$m P=2000N (a) Vertical cracked shaft deflection (b) Rotor response orbit, (c) X-Lateral frequency signal (d) Y-Lateral frequency signal (e) X-Lateral power spectral density (f) Y-Lateral power spectral density.

An increase in amplitudes of vibration is observed with the cracked rotor passing via its one-half and first critical speed ($\omega_1 = 1917.88\,rpm$ and $\omega_2 = 3451.803\,rpm$). Contact between the rotor and the stator increases the rotor dynamic stiffness, and this increases the rotor critical speed. However the presence of crack decreases the stiffness and decreases the critical speed of the rotor (Fig. 7 (B) (a)).

Comparing the case of uncracked rotor with rub, the presence of a crack increased interactions between the rotor and stator as indicated in Fig. 7 (B) (b). It is noted that a significant rebound appears just after the interaction and it becomes quite redundant when the stiffness of the rotor is reduced by the severity of the defects in the shaft.

In Fig. 7 (B) (b) the orbit becomes quite disordered and the lateral motion is no longer multi-periodic. Rotor-stator rub also increased vibration level of the cracked rotor in the presence of an axial force. As a result multiple resonance peaks appear in the vibration waveform in Fig. 7 (B) (a).

Approximately periodic responses of rub appear in Figs. 7 (B) (c), (d). Harmonics of 1× order (29.21 Hz) are noted as in results reported by [16]. The FFT spectral plot also shows that the higher frequencies, e.g., 1×, get excited by unbalance in presence of rub.

The 2×, 3× … harmonics which represent the superhamonics frequencies peaks are mainly due to crack, and harmonics at 1/2×, and 4×, etc., arise due to rotor-stator rub, and axial force. These harmonics are clearly seen in FFT plot (in Figs. 7 (B) (c), (d)). Power Spectral Density (PSD) describing distribution of the power of time series with frequency is plotted in Figs. 7 (A) (e), (f) and (B) (e), (f). From power spectral distribution in Figs. 7 (A) and (B), the rotor-stator contact is obvious, although there exist some trivial interferences components (e.g., the encircled part by red line in Figs. 7 (A) (e), (f)) at a frequency 57.5Hz. The higher frequency is excited by rub and disappears once the rotor-stator contact ceases (Figs. 7 (B) (e), (f)) due to the dissipative energy distribution.

Comparing the orbital patterns of the cracked rotor rub in Figs. 7 (B) (a), (b), it can be concluded that, the size of the inside loop, the presence of multiple peaks of resonance and the orbital movements of the rotor passing via the first critical speed are totally different and can provide information on crack presence.

Examining the system response in the presence of a crack, peaks of successive amplitude indicating super harmonic resonance appear in Figs. 7 (B) (c), (d).

The size of the inside loop is drastically affected by the crack and the rub. So, the orbital changes of the rotor via one-half of the first critical speed can be used as an indicator of a transverse crack, and the bounces inside the loops can be assigned as rub signature.

X. Rotor-Stator-Rub and Crack in 4 D.O.F

The fully coupled torsional, lateral vibrations of the unbalanced rotors with rub and a transverse crack and axial force are investigated, using the model referred by (28). Parametric resonance occurs in an axially loaded shaft when the excitation frequency is great than the shaft bending natural frequency ω_L as in [7]. Torsional resonance occurs when the angular velocity of the rotating shaft equals the torsional natural frequency ω_T.

Simulation of the rotor response using the torsional lateral-rotor model is made under fourth hypothesis.

For the first hypothesis the system response is simulated when the axial force is exerted and without rub. The torsional and lateral natural frequencies are then equal, $\omega_T = \omega_L$. And in the second hypothesis rotor is operated only with presence of crack and axial force.

The third and fourth is considering both rub-crack effect for which the torsional resonance behaviour takes places when $\omega_T \gg \omega_L$.

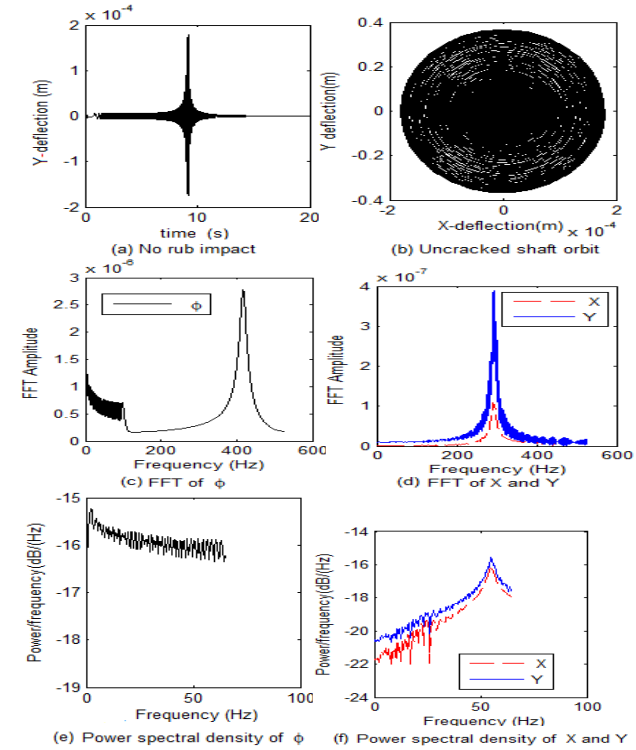

Fig. 8 (A) Dynamics system response from lateral-torsional-rotor model, no rub, no crack $\Delta K_\xi/K_b$=0. P=2000N, $\psi \neq 0$, $\omega_T = \omega_L$ (a) Vertical shaft deflection (b) Rotor response orbit (c) Torsional frequency signal (d) Lateral and frequency signal (e) Torsional power spectral density (f) Lateral power spectral density

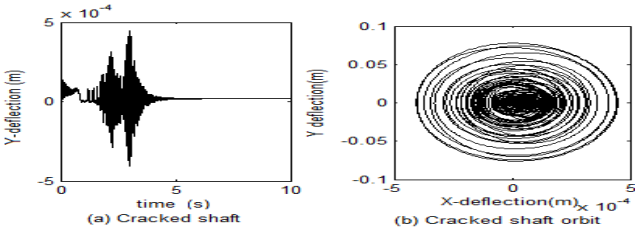

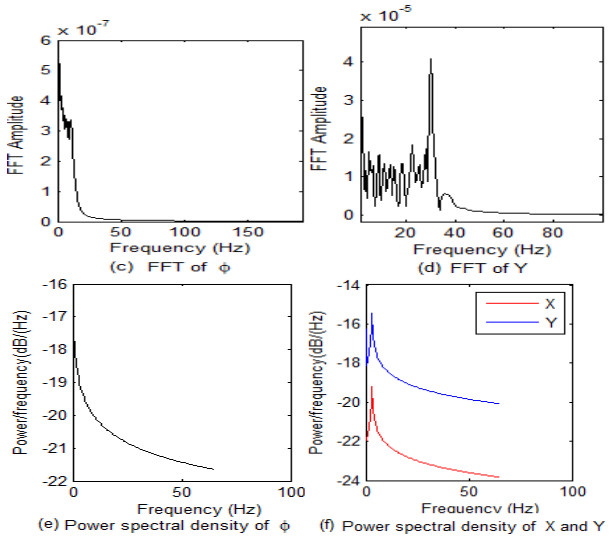

Fig. 8 (B) Dynamics system response using the lateral-torsional-rotor model, no rub, $\Delta K_\xi/K_b$=0.9542, P=2000N, $\psi \neq 0$; $\omega_T = \omega_L$ (a) Vertical shaft deflection (b) Rotor response orbit (c) Torsional frequency signal (d) Lateral and frequency signal (e) Torsional power spectral vibration. (f) Lateral power spectral density

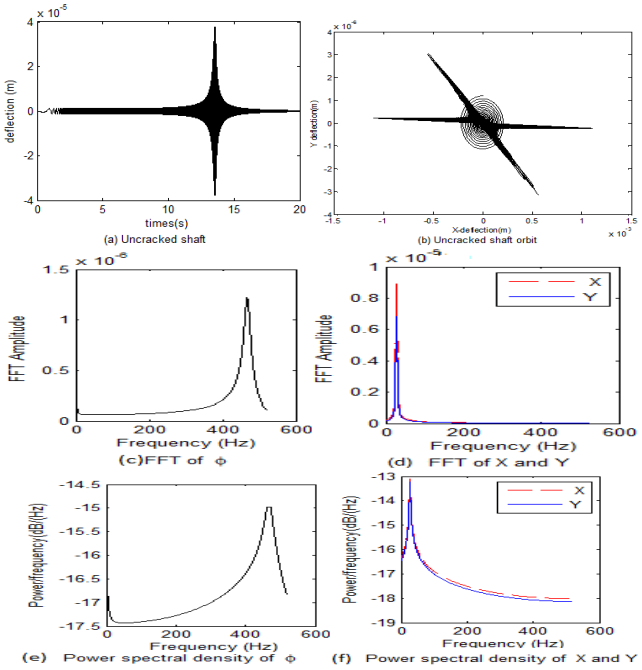

Fig. 9 (A) Dynamics response, with rotor-to-stator-rub and axial force but no crack $\Delta K_\xi/K_b$=0. P=2000N,$\Delta = 2.65 \times 10^{-7}$m (a) Vertical cracked shaft deflection (b) Rotor response orbit, (c) Torsional frequency signal domain, (d) Lateral frequency signal domain (e) Torsional power spectral vibration. (f) Lateral power spectral density

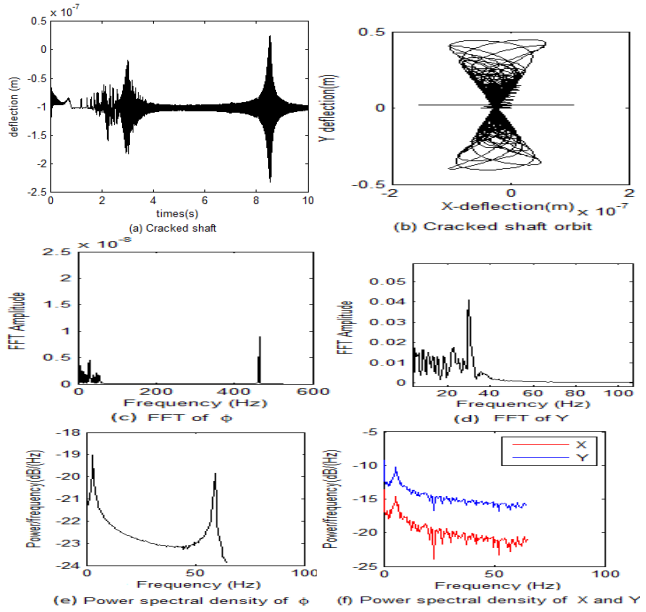

Fig. 9 (B) System response with, rub-crack, axial force: $\Delta K_\xi/K_b$=0.9542. P=2000N,$\omega_T \gg \omega_L$,$\Delta = 2.65 \times 10^{-7}$m (a) Vertical cracked shaft deflection (b) Rotor orbit response (c) Torsional frequency signal (d) Lateral frequency signal (e) Torsional power spectral density (f) Lateral power spectral density

Fig. 8 (A) (a) shows the synchronous rotor lateral response as a function of time. The shaft attains critical speed at 2042, 4 rpm indicated by peak amplitude in Fig. 8 (A) (d). The variation in FFT amplitude with frequency is plotted in Figs. 8 (A) (c), (d).

As noted in Figs. 8 (A) (c), (d) and 9 (A) (c), (d) once the critical speed is traversed, the amplitude of vibration decreases. This indicates that only unbalance and axial force are the source of the above vibrations.

This is verified by the orbit shape depicting a compressed circular response due to the large axial force and the synchronous response shown in the spectral plots in Figs. 8 (A) (f) and 9 (A) (f).

Spectral plots of the signal in Figs. 8 (B) (d) and 9 (B) (d) show an increase in the magnitude of frequency components before resonance; while it indicates a reduction in the magnitude of the second harmonic and a disappearance of higher frequency components. Fig. 9 (B) (b) shows the second rigid mode shapes of the modelled rotor. Presence of the second rigid mode can be attributed to multiple factors such as the model anisotropy, the higher axial force, the transient vibration which follows the removal of the friction torque in the rub free zone and the presence of the flexibility of the cracked shaft.

Analysis of the orbit presented in Fig. 9 (A) (b) revealed as noted already in [7], that the direction of the two maximum responses changes due to anisotropy model of rotor. Unlike the orbit of the cracked rotor describes the deflection shape of the system due to vibration and to local flexibility of the rotor at the damage location.

Figs. 8 (B) (a) and 9 (B) (a) are waveforms registered respectively at a rotational speed of 2309.4 rpm and 4510.21 rpm.

Two high resonance points and three resonance points developed from the excitation between the torsional and lateral rotor. The first one is the ordinary resonance and the other two are situated at the median and high resonance in Fig. 9 B (a).

Two possible factors could lead to the appearance of vibration peaks bands. The first is the large axial force and friction which are, of course, a consequence of rub. The axial force contributes to increased bending shaft effects, which accentuates the rotor-stator contact. However, friction forces cause a frictional torque opposite to rotor motion, resulting in a fluctuation of rotor speed.

Therefore, the frequency spectrum (Fig. 9 (B) (e)) would contain a vibration component corresponding to these modified processional speeds.

From Fig. 9 (B), it seems that axial force, crack and rub force have a big effect on the vibration response in comparison to the case of no rub-crack vibrations in Fig. 8 (A).

Examining the maximum power spectral density and shaft trajectory obtained for a cracked rotor, an increase in the spectral power density at half the critical speed can be used to diagnose presence of a breathing transverse crack.

XI. Conclusion

A study on coupled torsional-bending vibrations of an unbalanced rotor-stator system with rub is presented.

The results clearly indicate the change both in the orbit and the amplitude of the 1× harmonic components around one-half of the first critical speed.

An analytical model of an extended Jeffcott rotor is derived from Energy Principle accounting for lateral-torsional vibration coupling mechanism induced by an axial force and a "breathing" transverse crack.

Three cases are considered in this work; a model accounting for rotor-stator rub, a breathing transverse crack, and the parametric effect due to the axial compressive force applied opposite to motor.

A frequency response analysis to identify the frequencies of critical speeds has been done.

It is apparent that the axial force is a factor to take into account, its effect on the system vibration response in the presence of a crack is considerable. For a large axial force, the cracked rotor gives a chaotic behaviour and fault features become indiscernible in the vibration response.

When the excitation frequency is higher than the natural frequency, the second harmonic coincides with the natural frequency resulting in the amplitude amplification at that frequency.

Uncracked rotor gives a pure harmonic signal at the excitation frequency while a cracked rotor indicates harmonic frequency excitation due to the nonlinear behaviour of stiffness.

In time and frequency domain stronger higher harmonic components in the horizontal direction than in the vertical direction during passage via sub-harmonic resonances is observed. The increase in spectral power density at half the critical speed can serve as an additional indicator of a transverse breathing crack.

Acknowledgment

Support by the Department of Mechanical Engineering, VUT towards this work is highly acknowledged by the authors.

References

[1] T.H. Patel, and A.K. Darpe, Coupled bending torsional vibration analysis of rotor with rub and crack, Journal of Sound and Vibration Vol.326, 2009, pp 740–752.

[2] F. CHU, and W. LU, Determination of the rubbing location in a multi-disc rotor system by means of dynamic stiffness identification. Journal of sound and vibration, 2001. 235-246.

[3] G. Litak, and J. T. Sawicki, Intermittent behaviour of a cracked rotor in the resonance region, Chaos, Solutions and Fractals, 2009, 42, 1495-1501.

[4] R. Gasch, A Survey of the Dynamic Behaviour of a Simple Rotating Shaft with Transverse Crack, Journal of Sound and Vibration, 1993, 160(2): 313-332

[5] J.T. Sawicki, A. K. Sen, and L. Grzegorz, Multiresolution Wavelet Analysis of the Dynamics of a Cracked Rotor International Journal of Rotating Machinery, 2009.

[6] R.F. Beatty, Differentiating Rotor response due to radial rubbing, Journal of Vibration, Acoustics, Stress ,and Reliability in Design Vol107, 1985, pp151–160.

[7] B. O. Al-bedoor, Transient torsional and lateral vibrations of unbalanced rotors with rotor-to-stator rubbing. Journal of Sound and vibration 229(3), 2000, 627-645.

[8] J.T. Sawicki, J. Padovan, and R. Al-Khatib, The Dynamics of Rotor with Rubbing. International Journal of Rotating Machinery 1999, Vol. 5, No. 4, 1998, pp. 295-304.

[9] J.T. Sawicki, X. Wu, G. Y. Baaklini, and A. L. Gyekenyesi, "Vibration-based crack diagnosis in rotating shafts during acceleration through resonance," in Nondestructive Evaluation and Health Monitoring of Aerospace Materials and Composites II, vol. 5046 of Proceedings of SPIE, 2003, pp. 1–10, San Diego, Calif, USA.

[10] Y. B. Kim, and S.T. Noah, Bifurcation analysis for modified Jeffcott rotor with bearing clearances, Nonlinear Dynamics Vol. 1, 1990, pp 221-241.

[11] F. CHU, and W. LU, Stiffening effect of the rotor during the rotor-to-stator rub in a rotating machine, Journal of Sound and Vibration Vol.308, 2007, pp 758–766.

[12] R. Sukkar, and A.S. Yigit, Analysis of fully coupled torsional and lateral vibrations of unbalanced rotors subject to axial loads. Kuwait J.Sci.Eng.35 (2B), 2008, pp. 143-170.

[13] I. Mayes, W. Davies, The vibration behavior of a rotating shaft system containing a transverse crack. Vibration in rotating machinery, Inst. Mech, E, 1976, p.53-65.

[14] A.S. Sekhar, Crack identification in a rotor system: a model- based approach. Journal of sound and vibration 270, 2004, 887-920.

[15] A.S. Yigit, and A.P. Christoforou, Coupled Torsional and Bending Vibrations of Actively Controlled Drillstings. Journal of Sound and Vibration, 2000, 234: 67-83.

[16] A.K.Darpe, Dynamics of cracked rotor. PhD Thesis, IIT Delhi, 2000.